LAWRENCE
LIVERMORE
NATIONAL
LABORATORY

UCRL-PROC-231029

X-ray Thomson Scattering from Dense Plasmas

S. H. Glenzer

May 18, 2007

ATOMIC PROCESSES IN PLASMAS
GAITHERSBURG, MD, United States
March 19, 2007 through March 22, 2007

X-ray Thomson Scattering from Dense Plasmas

S. H. Glenzer

Lawrence Livermore National Laboratory, L-399, University of California, P.O. Box 808, Livermore, CA 94551, USA

Abstract. X-ray Thomson scattering has been developed for accurate measurements of densities and temperatures in dense plasmas. Experiments with laser-produced x-ray sources have demonstrated Compton scattering and plasmon scattering from isochorically-heated solid-density beryllium plasmas. In these studies, the Ly-alpha or He-alpha radiation from nanosecond laser plasmas has been applied at moderate x-ray energies of E = 3 - 9 keV sufficient to penetrate through the dense plasma and to avoid intense bremsstrahlung radiation at lower energies. In backscattering geometry, the experiments have accessed the non-collective Compton scattering regime where the spectrum reflects the electron velocity distribution of the plasma, thus providing an accurate measurement of the temperature. In addition to the inelastic Compton scattering feature, the spectra also show elastic (Rayleigh) scattering from tightly bound electrons. The intensity ratio of these features yields the ionization state that has been applied to infer the electron density in isochorically-heated matter. Forward scattering in these conditions have observed plasmons that allow a direct and accurate measurements of the electron density from the frequency shift of the plasmon peak from the incident probe energy. The back and forward scattering data are in mutual agreement indicating an electron density of $n_e = 3 \times 10^{23}$ cm^{-3}, which is also consistent with results from radiation hydrodynamic simulations. These findings indicate that x-ray Thomson scattering provides accurate characterization in the previously unexplored regime of high-energy density matter. Future work will explore applications to measure compressibility, collisions, and electronic properties of dense matter.

Keywords: Plasma Diagnostic, Dense Plasmas, Thomson scattering.
PACS: 52.25.Os, 52.35.Fp, 52.50.Jm

INTRODUCTION

Accurate characterization techniques of dense plasmas for measurements of temperature, density, and ionization state are important for understanding and modeling high-energy density science experiments.[1,2] Examples of important applications include the measurement of the electron temperature of in inertial confinement fusion capsule implosions where the ratio of electron to Fermi temperature will characterize the fuel adiabate.[3] Moreover, x-ray scattering may be applied as a tool to resolve fundamental physics questions such as the equation of state in dense matter[4], structure factors in two-component plasmas[5], limits of the validity of the random phase approximation[6], and the role of collisions.[7]

Significant advances in the physics of low-density plasmas has been enabled by the development of optical lasers and the ability to characterize the plasma conditions with Thomson scattering.[8-10] Ultraviolet lasers[11,12] and soft x-ray lasers[13] have been subsequently applied to characterize high-density laser-produced plasmas by Thomson

scattering[14-17] and interferometry[18,19], respectively. However, to access dense matter with densities of solid and above it has been necessary to develop powerful x-ray sources[20] that penetrate through dense or compressed materials[21] and that fulfill the stringent requirements[22] on photon numbers and bandwidth for spectrally-resolved x-ray Thomson scattering measurements in single shot experiments.[23]

In this work, laser-produced He-alpha and Ly-alpha x-ray sources have been applied to perform x-ray Thomson scattering measurements in isochorically-heated solid-density beryllium.[24,25] Measurements in backscatter geometry have accessed the Compton scattering regime where the scattering process is non-collective and the spectrum shows the Compton down-shifted line that is broadened by the thermal motion of the electrons, thus providing the temperature with high accuracy. In addition to the Compton scattering feature from inelastic scattering by free and weakly bound electrons, the non-collective scattering spectrum exhibit the unshifted Rayleigh scattering component from elastic scattering by tightly bound electrons. The latter occupy quantum states with ionization energy larger than the Compton energy deep in the Fermi sea that cannot be excited due to the Pauli exclusion principle. These electrons become available for inelastic scattering by x rays and contribute to the Compton feature by thermal excitation and ionization. The intensity ratio of the inelastic Compton to the elastic Rayleigh scattering component can hence be a sensitive measure of the ionization state.[24,26,27] In isochorically heated matter where the ion density is known *a priori*, the ionization state also provides a measurement of the electron density.

In the forward scattering regime, the collective plasmon oscillations have been observed.[25] The spectrum provides directly the local electron density from the frequency shift of the plasmon peak from the incident probe x-ray energy. The experiments have been performed in the well-characterized, isochorically-heated, solid-density beryllium target platform. Forward scattering of the narrow-band chlorine Ly-alpha x-ray line at 2.96 keV accesses the collective scattering regime and measures the characteristic plasmon peak associated with the collective plasma (Langmuir) oscillations.[28] The results show that this technique provides densities in agreement with the Compton scattering method that is also consistent with radiation hydrodynamic calculations using the code LASNEX.[29] In addition, forward scattering is not dependent on knowledge of the ion density and is directly applicable to characterize compressed matter.

THEORY OF X-RAY THOMSON SCATTERING

For conditions where the energy of the scattered radiation is close to the incident x-ray probe energy, E_0, i.e., for small momentum transfers, the scattering geometry and the probe energy determine the scattering vector **k** through the relation

$$k = |\mathbf{k}| = 4\pi \frac{E_0}{hc} \sin\left(\frac{\theta}{2}\right). \quad (1)$$

In collective scattering the probe samples plasma scale lengths larger than the plasma screening length, λ_S, which can be approximated by the Thomas-Fermi length, λ_{TF}, for a degenerate system. For classical plasmas, on the other hand, the usual

Debye screening length, $\lambda_D = (\varepsilon_0 k_B T_e / n_e e^2)^{1/2}$, should be applied. Here, ε_0 is the permittivity of free space, k_B is the Boltzmann constant, T_e is the electron temperature, and n_e is the electron density. For weakly degenerate plasmas, calculating the Debye length at an effective temperature will result in a smooth interpolation between the degenerate and classical plasma limits.[30,31]

In the collective scattering regime, the scattering parameter $\alpha>1$ with α being defined as

$$\alpha = \frac{1}{k\lambda_S}. \tag{2}$$

For example, to access collective scattering in a weakly degenerate solid-density beryllium plasma with electron temperature of the order of the Fermi temperature, $T_e = T_F = 15\text{eV}$, requires forward scattering with $\theta = 40^\circ$ and x-ray probe energies or order $E_0 = 3\text{keV}$. In these conditions, the scattering is predominantly probing *k*-vectors with $k = 10^{10}\ \text{m}^{-1}$. Calculating the screening length at the effective temperature results in $\alpha = 1.6$. In this regime, the scattered light spectrum shows collective effects corresponding to scattering resonances off ion acoustic waves and off electron plasma waves, i.e. plasmons. The plasmon frequency shift from E_0 is determined by the plasmon dispersion relation that can be approximated for small values of *k* by[32]

$$\omega_{plasmon}^2 = \omega_p^2 + 3k^2 v_{th}^2 (1 + 0.088 n_e \Lambda_e^3) + \left(\frac{\hbar k^2}{2m_e}\right)^2. \tag{3}$$

where $\omega_p^2 = (n_e e^2/\varepsilon_0 m_e)^{1/2}$ is the plasma frequency, $v_{th} = (k_B T/m_e)^{1/2}$ is the thermal velocity and $\Lambda_e = h/(2\pi m_e k_B T)^{1/2}$ is the thermal wave length. In Eq. (3), the first term is a result of electron oscillations in the plasma, the second term represents the effect on propagation of the oscillation from thermal pressure. The third term includes degeneracy effects from Fermi pressure, and the last term is the quantum shift.[33] The quantum shift and the electron oscillation terms are temperature independent and account for most of the plasmon shift. Therefore, the plasmon energy provides a sensitive measure of the plasma electron density.

In backscattering geometry and at high x-ray probe radiation energies, the momentum transfer during the scattering process results in a significant frequency shift to the scattered radiation, i.e. the Compton effect.[34] During the scattering process, the incident photons transfer the momentum $\hbar k$ and the energy $\hbar\omega = \hbar^2 k^2 / 2m_e$ to the electrons. Momentum and energy can only be transferred to the free electrons and weakly bound electrons with binding energy less than the Compton energy. The free electrons carry the information on the temperature of the plasma resulting in a spectral broadening, $\omega = \mathbf{kv}$. The spectrum directly reflects the distribution function showing a parabolic function in case of a degenerate plasma with the width reflecting the Fermi temperature, T_F, and in case of a classical plasma a Gaussian spectral profile indicates a Maxwell-Boltzmann distribution function with the width providing the electron temperature, T_e.

On the other hand, bound electrons with ionization energies larger than Compton energy cannot be excited, and no energy can be transferred during the scattering process. The corresponding spectral feature is an un-shifted elastic scattering component. Clearly, with increasing ionization tightly bound electron become

available for inelastic Compton scattering, and the ratio of elastic to inelastic scattering is a measure of the ionization state. In isochoric heated matter, the electron density can be deduced with $n_e = 6 \times 10^{23}$ Z/A ρ cm^{-3} with ρ = 1.85 for Be, and for Z = 2.5 resulting in $n_e = 3 \times 10^{23}$ cm^{-3}.

The scattering cross section is described in terms of the dynamic structure factor of all the electrons in the plasma[30,35,36]

$$\frac{d^2\sigma}{d\Omega d\omega} = \sigma_{Th} \frac{k_1}{k_0} S(\mathbf{k},\omega) \tag{4}$$

where σ_{Th} is the usual Thomson cross section and $S(\mathbf{k},\omega)$ is the total dynamic structure factor defined as

$$S(\mathbf{k},\omega) = \left| f_I(k) + q(k) \right|^2 S_{ii}(\mathbf{k},\omega) + Z_f S_{ee}^0(\mathbf{k},\omega) + Z_C \int S_{ce}(\mathbf{k},\omega-\omega') S_s(\mathbf{k},\omega') d\omega'. \tag{5}$$

The first term in Eq. (5) accounts for the density correlations of electrons that dynamically follow the ion motion. This includes both the core electrons, represented by the ion form factor $f_I(k)$ and the screening cloud of free (and valence) electrons that surround the ion, represented by $q(k) = \sqrt{Z} S_{ei}/S_{ii}$. $S_{ei}(\mathbf{k},\omega)$ and $S_{ii}(\mathbf{k},\omega)$ are the electron-ion and the ion-ion structure factors, respectively. This term accounts for the scattering peak around the incident x-ray probe energy E_0. Its spectral features cannot be resolved in present experiments that use laser-produced x-ray sources and is conveniently labeled ion feature or elastic scattering feature.

The k=0, $T_e = T_i$ limit is indeed known $S_{ii}(k=0,\omega) = (\gamma_i + Z_f)^{-1}$ with γ_i being the compressibility ratio (γ_i =1 for an ideal gas) and Z_f is the ionization state. For the experiments in isochorically heated beryllium, applying this limit overestimates the intensity of the ion feature relative to the intensity of the plasmon. This finding is also observed for more detailed analytical calculations.[37] Thus, detailed hypernetted chain calculations with quantum interaction potentials have been developed.[38] Several quantum interaction potentials may be applied to provide accurate estimates of the intensity of the ion feature.[39-42]

The second term in Eq. (5) calculates the contribution to the scattering spectrum from the free electrons that do not follow the ion motion. Here, $S_{ee}(\mathbf{k},\omega)$ is the high frequency part of the electron-electron correlation function[43] and it reduces to the usual electron feature[44] in the case of an optical probe. Under the assumption that inter particle interactions are weak, so that the nonlinear interaction between different density fluctuations is negligible, the dielectric function may be derived in the random phase approximation (RPA)[45,46] that includes the Compton shift but is not including corrections to describe scattering from strongly coupled plasmas. More recent improvements apply Memin theory[47,48] including the effect of collisions. Several approximation are available for the dynamic collision frequency[7,49] that primarily affect the damping, i.e., the spectral width of plasmons in collective scattering. These models may be tested with simultaneous measurements of plasmons and the electron temperature. Compton backscatter measurements or detailed balance that affects the intensity ratio of down- and up-shifted plasmons may be applied for this purpose.[50]

The last term of Eq. (5) includes inelastic scattering by core electrons, which arises from Raman transitions to the continuum of core electrons within an ion,

$S_{ce}(\mathbf{k},\omega)$modulated by the self-motion of the ions, represented by $S_s(\mathbf{k},\omega)$. The corresponding spectrum of the scattered radiation is that of a Raman-type band. For experiments with isochorically-heated beryllium, we find that this contribution is small compared to the free electron dynamic structure.

X-RAY THOMSON SCATTERING EXPERIMENTS

Solid-density matter has been characterized by spectrally-resolved x-ray scattering more than 70 years ago.[51] These data have observed the Fermi distribution for cold solids predicted by Chandrashekar.[52] For the characterization of warm dense matter, the integrated total scattering has been measured as function of scattering angle[21] before the first x-ray Thomson scattering have been performed on the Omega laser facility yielding spectrally resolved x-ray scattering spectra in the high-energy density physics regime.[24,25]

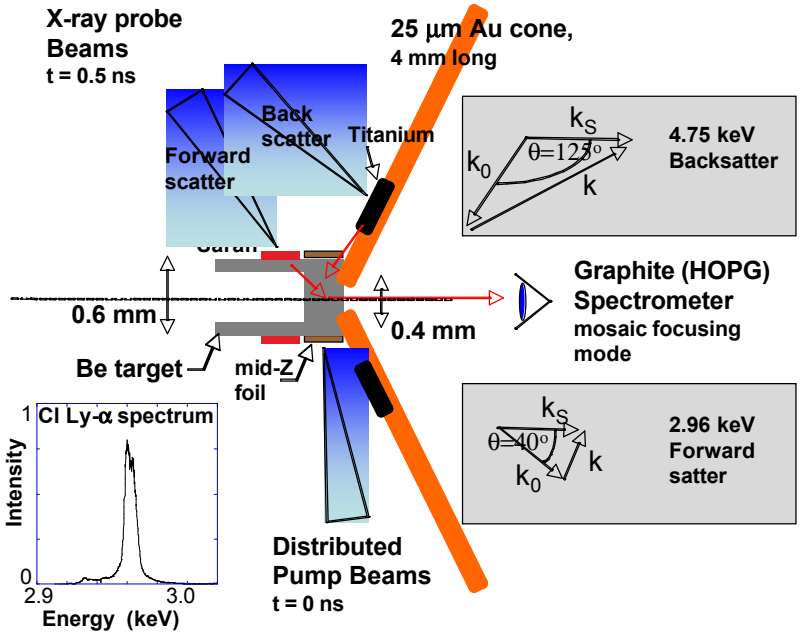

FIGURE 1. Schematic of scattering experiments employing the titanium He-alpha spectral line in backscattering at θ = 125° or the chlorine Ly-alpha line in forward scattering at θ = 40°. The inset shows a Ly-alpha source spectrum. The k-vector diagrams show the averaged scattering vectors in both geometries yielding non-collective or collective scattering. Up to 15kJ of laser energy has been used for the broadband L-shell heating radiation and up to 7 kJ to produce the narrowband x-ray probe radiation.

Figure 1 shows a schematic of backward and forward scattering experiments on isochorically-heated solid-density beryllium. The beryllium is homogeneously and isochorically heated by L-shell x-rays from a mid-Z foil (Rh or Ag wrapped around the Be) and the dense plasma is probed after t = 0.5 ns with the narrowband x-ray probe radiation from titanium of chlorine. The high laser energy for producing the narrow band x-ray probe and the broadband heating radiation provides sufficient photons for producing homogeneous warm dense states of matter and probing in single shot experiments.

The scattered x rays have been observed through a 400 microns diameter diagnostic hole cut in the center of a 4 mm large Au shield. A gated Bragg crystal spectrometer has been employed in the mosaic focusing mode only observing x-rays scattered from

the central homogeneously heated beryllium. The Au shield prevented a direct view of the source of the probe x rays or scattered radiation from shock waves. For a conversion efficiency of laser energy into resonance line radiation of 4 x 10^{-3}, a solid angle of beryllium plasmas that is probed of 10^{-2}, and 7kJ of laser energy, a total of 0.1J of probe x-rays or 10^{14} titanium He-alpha x-ray photons are provided at the beryllium plasmas for the duration of the detector gating time of 0.3 ns. The scattering fraction is $\sigma_{Th} n_e L = 3 \times 10^{-3}$ for a 0.4 mm long plasmas viewed by the spectrometer and the collection fraction is 0.1 rad x 1 mrad x 1% / $4\pi \approx 10^{-7}$. Thus, 30,000 photons are detected in a single shot.

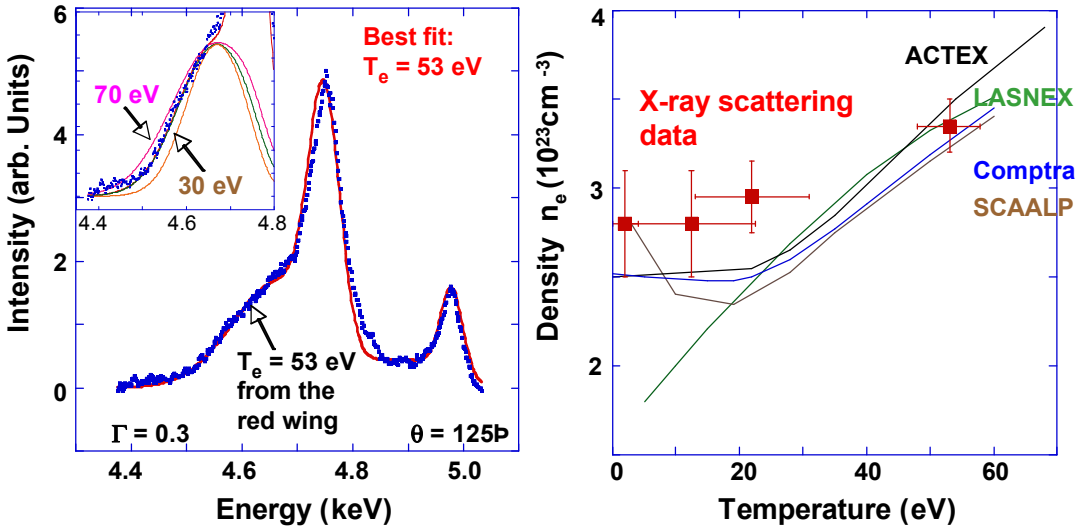

FIGURE 2. Scattering spectrum (blue dots) from isochorically heated beryllium shows elastic and inelastic (Compton) scattering components from titanium He-alpha and Ly-alpha probe x rays (left). The spectrum is fit well with the dynamic structure factor (red line) proving a temperature of T_e = 53 eV and density of $n_e = 3.3 \times 10^{23}$ cm^{-3}. These results have tested ionization balance calculations in the solid density plasma regime (right).

Figure 2 shows an example of a back-scattering spectrum from heated beryllium. Elastic scattering from both the titanium He-alpha radiation at 4.75 keV and Ly-alpha radiation at 4.96 keV is observed together with the downshifted Compton scattering feature. The spectrum is fit by the dynamic structure factor, Eq. (5), providing temperatures and densities from the broadening of the Compton downshifted line and from the intensity ratio of elastic and inelastic scattering components. The inset shows the sensitivity of the shape of the red Compton scattering wing to the electron temperature; T_e is inferred from these data with an accuracy of 10%.

A similar analysis has been performed when inferring the ionization state and density from the intensity ratio.[24,35] In conditions without weakly bound electrons the intensity of the inelastic scattering component is solely determined by the free electrons yielding the density with accuracy of about 10%. For lower temperature conditions, however, where bound electrons scatter non-elastically the contributions from free and weakly bound electrons blend. Nonetheless, the bound-free spectrum is well known and can be distinguished from the Compton scattering spectrum of the

free electrons yielding temperature and density information with larger error bars of about 30-50%.

In the experiment, the temperature of the beryllium plasma has been varied by using different mid-Z foils, i.e. Mo, Rh, and Ag, to convert the laser energy to L-shell heating x rays. In addition, on some shots only half of the laser energy per beam was applied probing a temperature phase space of up to T_e = 53 eV. At the highest temperatures, we observe that the measured electron density agrees with various ionization balance models, i.e., the codes ACTEX[53], Comptra[54], LASNEX[29] and SCAALP.[55] On the other hand, at lower electron temperatures, the role of delocalized electrons requires the calculation of all possible interactions between the plasma constituents including the screening of the bound states.[53] For large densities, the classical Debye-Hückel (Yukawa) potential needs to be replaced by quantum interaction potentials that approach the thermal de Broglie wavelength. This allows the calculation of the number of electrons that are no longer bound to a single ion. These electrons are free or weakly bound like the conduction electrons in a metal. Calculations that use interpolation functions between the zero and high temperature conductivity limits show deviations from the measured data are small temperatures.[55] This regime requires additional characterization of the physical properties, e.g., by using measurements at smaller scattering angles and lower x-ray energy to approach the collective regime, cf. Fig. 1.

Figure 3 shows experimental scattering spectra from isochorically heated beryllium measured in forward scattering of the chlorine Ly-alpha line at 2.96 keV.

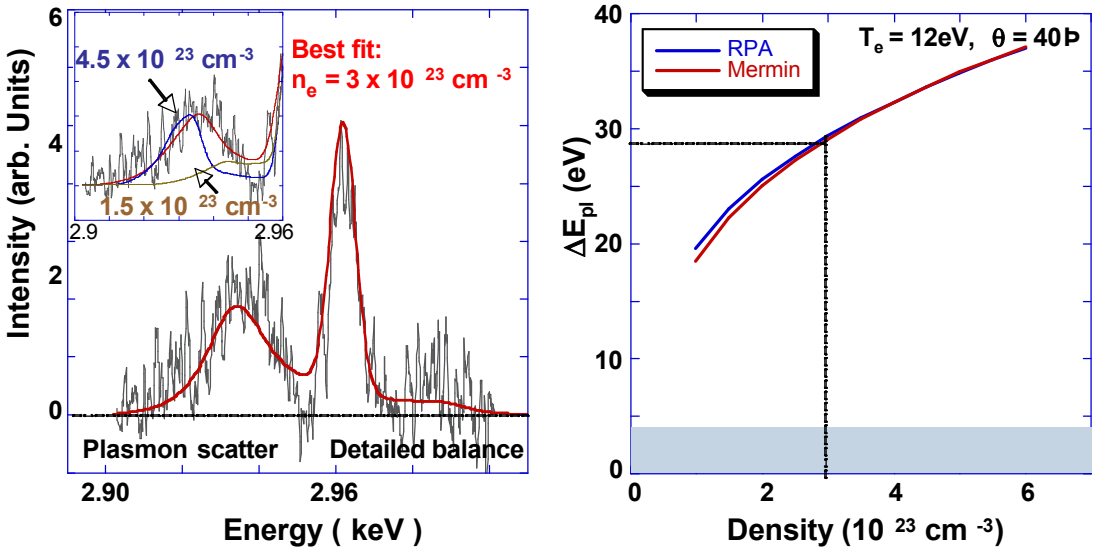

FIGURE 3. Forward scattering spectrum (black line) from isochorically heated beryllium shows elastic and inelastic (plasmon) scattering from chlorine Ly-alpha probe x rays (left). The spectrum is fit well with the dynamic structure factor (red line) proving a temperature of T_e = 12 eV and density of n_e = 3 x 10^{23} cm^{-3}. The dispersion relation for plasmons determines the frequency shift of the plasmon from the incident x-ray probe radiation yielding the electron density (right).

To resolve the plasmon frequency shift and damping in forward scattering, the x-ray bandwidth has to be smaller compared to the Compton scattering measurements. In Figure 3, the plasmon shift of ΔE = 28 eV was resolved by the chlorine Ly-alpha

probe radiation with an effective bandwidth of 7.7 eV and no significant dielectronic satellite radiation on the red wing of the Ly-alpha doublet, see Fig. 1 (inset). Also shown are synthetic scattering profiles that represent a convolution of the theoretical form factor $S(\mathbf{k},\omega)$, calculated for the range of **k**-vectors of the experiment, with the spectral resolution of 7.7 eV. The ion feature is observed as an elastic scattering peak at E_0 that is not resolved in this experiment. On the lower-energy wing of the ion feature we observe a strong plasmon resonance. On the higher-energy wing with nearly the same frequency shift, the data show a weak up-shifted plasmon signal. Compared to the intensity of down-shifted plasmon, the intensity is reduced by the Bose function $e^{-\hbar\omega/k_B T_e}$ reflecting the principle of detail balance. The intensity ratio of these plasmon features is thus sensitive to the temperature. In the present experiment, the signal to noise ratio only allows us to deduce an upper limit of $T_e < 25$ eV.

In $S(\mathbf{k},\omega)$, collision effects on plasmons is accounted for with a Mermin ansatz thus accounting for weak degeneracy effects. While the frequency shift is only marginal affected we observe that collisional damping cannot be neglected. The fit provides a temperature of 12 eV and density of $n_e = 3 \times 10^{23}$ cm^{-3}. Figure 3 (right) indicates that the density is accurately determined by the shift of the plasmon. For the small **k**-vectors probed in the present experiment, significant deviations from the random phase approximation are not expected yielding an error bar in density that is solely determined by the signal to noise ratio and the quality of the fit. The inset in Fig. (3) shows calculations for densities of 1.5×10^{23} cm^{-3} and 4.5×10^{23} cm^{-3} indicating that the error bar in density is of order 20% in the present experiment; a value that may be improved with better signal to noise ratio.

Inferring the temperature from the collective scattering spectrum requires accurate measurements of the up-shifted plasmon and the application of detailed balance or alternatively the width of the plasmon may be used. The latter is determined by Landau damping and collisional damping.

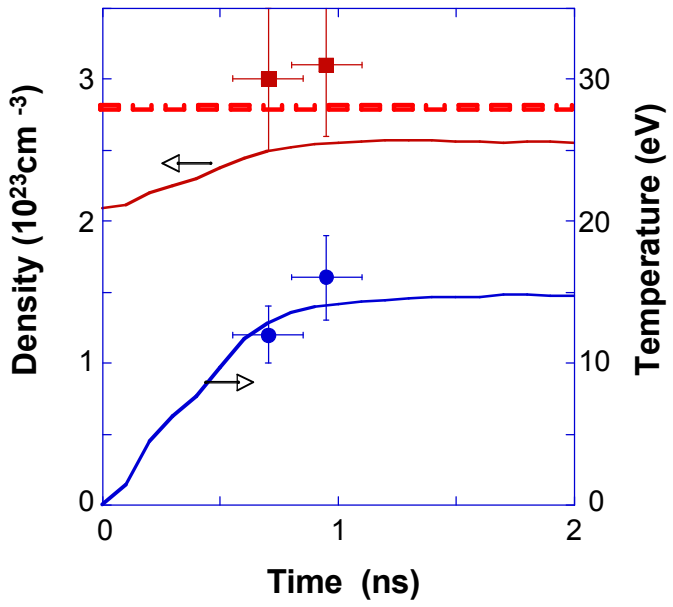

FIGURE 4. Plasma parameters from collective x-ray scattering and radiation hydrodynamics calculations are shown. The dashed curve shows the electron density for solid-density beryllium for Z = 2.3 measured in backscattering. The calculated density agrees marginally with the data from forward and backward scattering due to approximations in the calculation of Z in hydrodynamic modeling.

For our conditions, collisions account for an additional broadening of approximately 5 eV. The difference can be as large as a factor of 1.5 for scattering

spectra calculated at a single scattering angle. Clearly, scattering experiments in a regime where damping by collisions dominates the broadening of plasmons are of interest to test models of the collisionality in dense plamas. For the experiments discussed here, collisions provide a correction to the measured width. A good fit of the plasmon spectrum is obtained for a temperature of 12 eV and with the dynamic collision frequency calculated in Born approximation.

Figure 4 shows the experimental results from the forward scattering experiments. The temperature is lower in these data because 1) the detector was gated earlier during the heating of the plasma, 2) fewer laser beams have been used to illuminate the L-shell converter, and 3) a higher-Z element was used, i.e. Ag. Calculations show 20-30% lower conversion efficiency than for Rh or Mo. We find that the experimental temperature data agree well with radiation hydrodynamic simulations. In addition, the density is in good agreement with the expectations from the backward scattering experiments in the low temperature range, cf. Fig. (2) indicating that the plasmon spectrum provides a robust density diagnostics.

CONCLUSIONS AND OUTLOOK

X-ray Thomson scattering experiments on isochorically heated solid-density beryllium have shown accurate characterization of warm dense matter. Results from forward and backward scattering measurements have been shown to yield mutually consistent results. In particular, the electron density inferred from the frequency shift of plasmons agrees with the ionization balance measurements from the intensity ratio of the Compton scattering to elastic scattering component. Moreover, the electron temperature is inferred from the spectrum of the Compton downshifted line that is directly reflecting the electron velocity distribution providing temperatures from first principles. These results show that the x-ray scattering technique can be applied to measure the compressibility of dense matter from the plasmon frequency shift or in case of a degenerate system from the Compton scattering feature that will reflect the Fermi temperature. Future applications will include measurements of the conductivity from the collisional damping of plasmons and investigations of the validity of the random phase approximations at large values of the scattering vector k.

ACKNOWLEDGMENTS

This work was performed under the auspices of the U.S. Department of Energy by University of California Lawrence Livermore National Laboratory under contract No. W-7405-Eng-48. Supported by LDRD 05-ERI-003, SFB 652, and the Alexander-von-Humboldt society.

REFERENCES

1. J. D. Lindl, P. Amendt, R. L. Berger et al. *Phys. Plasmas* **11**, 339 (2004).
2. B. A. Remington, P. R. Drake, D. D. Ryutov., *Rev. Mod. Physics* **78**, 755 (2006).
3. M A. Kritcher, P. Neumayer, M. K. Urry et al., *High Energy Density Physics* (2007), in print.
4. L. B. DaSilva et al. *Phys. Rev. Lett.* **78,** 483 (1997); M. D. Knudson et al., *ibid* **90,** 035505 (2003).

5. S. Ichimaru and S. Tanaka, *Phys. Rev. A* **32**, 1790 (1985).
6. G. Gregori, S. H. Glenzer, and O. L. Landen, *J. Phys. A* **36**, 5971 (2003).
7. H. Reinholz, R. Redmer, G. Röpke, and A. Wierling, *Phys. Rev. E* **62**, 5648 (2000).
8. H.-J. Kunze E. Fünfer, B. Kronast, and W. H. Kegel, *Phys. Lett*. **11**, 42 (1964).
9. A. A. Offenberger W. Blyth, A. E. Dangor et al., *Phys. Rev. Letters* **71**, 3983 (1993).
10. A W. DeSilva et al., *Phys. Fluids B* **4**, 458 (1992).
11. S. H. Glenzer T. L. Weiland, J. Bower et al., *Rev. Sci. Instrum*. **70**, 1089 (1999).
12. A. J. Mackinnon S. Shiromizu, G. Antonini et al., *Rev. Sci. Intrum* **75**, 3906 (2004).
13. J. Dunn, Y. Li, A. L. Osterheld et al., *Phys. Rev. Letters* **84**, 4834 (2000).
14. S. H. Glenzer, C. A. Back, K. G. Estabrook et al., *Phys. Rev. Letters* **77**, 1496 (1996).
15. S. H. Glenzer, W. Rozmus, B. J. MacGowan et al., *Phys. Rev. Letters* **82**, 97 (1999).
16. S. H. Glenzer, K. B. Fournier, B. G. Wilson et al., *Phys. Rev. Letters* **87**, 045002 (2001).
17. D. H. Froula, P. Davis, L. Divol et al., *Phys. Rev. Letters* **95**, 195005 (2005).
18. J. Filevich, J. J. Rocca, M. C. Marconi et al., *Applied Optics* **43**, 3938 (2004).
19. R. F. Smith, J. Dunn, J. Nilsen et al., *Phys. Rev. Letters* **89**, 065004 (2002).
20. O. L. Landen et al., *Rev. Sci. Instrum*. **72**, 627 (2001).
21. D. Riley et al., *Phys. Rev. Letters* **84**, 1704 (2000).
22. M. Urry, G. Gregori, O.L. Landen et al., *J. Quan. Spectr. Rad. Transfer* **99**, 636 (2006).
23. O. L. Landen, S.H. Glenzer, M.J. Edwards et al., *J. Quan. Spectr. Rad. Transfer* **71**, 465 (2001).
24. S. H. Glenzer, G. Gregori, R. W. Lee et al., *Phys. Rev. Letters* **90**, 175002 (2003).
25. S. H. Glenzer, O. L. Landen, P. Neumayer et al., *Phys. Rev. Letters* **98**, 065002 (2007).
26. S. H. Glenzer, G. Gregori, F. J. Rogers et al., *Phys. Plasmas* **10**, 2433 (2003).
27. G. Gregori, S. H. Glenzer, F. J. Rogers et al., *Phys. Plasmas* **11**, 2754 (2004).
28. L. Tonks and I. Langmuir, *Phys. Rev.* **33**, 195 (1929).
29. G. Zimmerman and W. Kruer, *Comments Plasma Phys. Controlled Fusion* **2**, 85 (1975).
30. F. Perrot and M. W. C. Dharma-Wadarna, *Phys. Rev. B* **62**, 15636 (2000).
31. M. W. C. Dharma-Wadarna and F Perrot, *Phys. Rev. Letters* **84**, 959 (2000).
32. R. Zimmerman, *Many-Particle Theory of Highly Excited Semiconductors* (Teubner, Leipzig, 1987).
33. F. Haas, G. Manfredi, and M. Feix, *Phys. Rev. E* **62**, 2763 (2000).
34. A. H. Compton *Phys. Rev* **21**, 483 (1923).
35. G. Gregori, S. H. Glenzer, W. Rozmus, R. W. Lee, O. L. Landen, *Phys. Rev. E* **67**, 026412 (2003).
36. J. Chihara, *J. Phys.: Condens. Matter* **12**, 231 (2000).
37. G. Gregori, S. H. Glenzer and O. L. Landen, *Phys. Rev. E* **74**, 026402 (2006).
38. V. Schwarz, Th. Bornath, W. D. Kraeft et al., *Contr. Plas. Phys.* (2007), in print.
39. Yu. L. Klimontovich and W. D. Kraeft, *High. Temp. Physics(USSR)***12** , 212 (1974).
40. G. Kelbg, *Ann. Phys. (Leipzig)* **12**, 219 (1963); **13**, 354 (1963); **14**, 394 (1964).
41. C. Deutsch, *Phys. Lett*. **60**A, 317 (1977).
42. A. V. Filinov, V. O. Golubnychiy, M. Bonitz et al., *Physical Review E* **70**, 046411 (2004).
43. S. Ichimaru, *Basic Principles of Plasma Physics* (Addison, Reading, MA, 1973).
44. E. E. Salpeter, *Phys. Rev.* **120**, 1528 (1960).
45. D. Pines and D. Bohm, Phys. Rev. **85**, 338 (1952). D. Pines and P. Nozieres, *The Theory of Quantum Fluids* (Addison-Wesley, Redwood, CA, 1990).
46. D. Kremp. M. Sclanges, W.-D. Kraeft and T. Bornath, *Quantum Statistics of Nonideal Plasmas* (Springer, Berlin 2005).
47. A. Höll, R. Redmer, G. Röpke, and H. Reinholz, Eur. Phys. J. D **29,** 159 (2004).
48. R. Redmer, H. Reinholz, G. Röpke et al., *IEEE Trans. Plas. Sci.,* **33**, 77 (2005).
49. R. Thiele et al., *J. Phys.. A* (2007), in print.
50. A. Höll, Th. Bornath, L. Cao et al., *High Energy Density Physics* (2007), in print.
51. J. W. M. DuMond, *Phys. Rev.* **29**, 643 (1929). J. W. DuMond and H. A. Kirkpatrick, *ibid* **37**, 136 (1931).
52. S. Chandrasekhar, *Proceedings of the Royal Society* A **125**, 231 (1929).
53. F. Rogers, *Phys. Plasmas* **7**, 51 (2000). . F. Rogers and D. A. Young, *Phys. Rev. E* **56**, 5876 (1997).
54. R. Redmer, *Phys. Rev. E* **59**, 1073 (1999). S. Kuhlbrodt and R. Redmer, *ibid* **62**, 7191 (2000).
55. P. Renaudin, C. Blancard, G. Faussurier, and P. Noiret, *Phys. Rev. Letters* **88**, 215001 (2002).